Article

Marked Dependence on Carrier-Ligand Bulk but Not on Carrier-Ligand Chirality of the Duplex versus Single-Strand Forms of a DNA Oligonucleotide with a Series of G–Pt(II)–G Intrastrand Cross-Links Modeling Cisplatin–DNA Adducts

Vladimir Beljanski, Julie M. Villanueva, Paul W. Doetsch, Giovanni Natile, and Luigi G. Marzilli

J. Am. Chem. Soc., **2005**, 127 (45), 15833-15842• DOI: 10.1021/ja053089n • Publication Date (Web): 25 October 2005

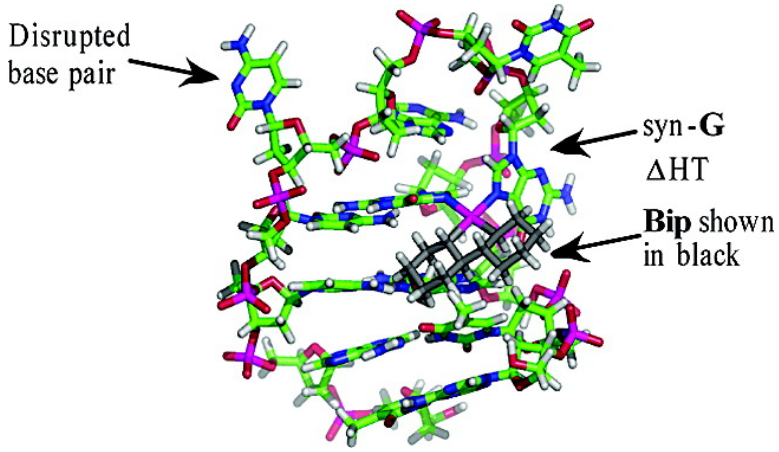

More About This Article

Additional resources and features associated with this article are available within the HTML version:

- Supporting Information
- Links to the 6 articles that cite this article, as of the time of this article download
- Access to high resolution figures
- Links to articles and content related to this article
- Copyright permission to reproduce figures and/or text from this article

View the Full Text HTML

J|A|C|S
ARTICLES
Published on Web 10/25/2005

Marked Dependence on Carrier-Ligand Bulk but Not on Carrier-Ligand Chirality of the Duplex versus Single-Strand Forms of a DNA Oligonucleotide with a Series of G−Pt(II)−G Intrastrand Cross-Links Modeling Cisplatin−DNA Adducts

Vladimir Beljanski,[§] Julie M. Villanueva,[§] Paul W. Doetsch,[‡] Giovanni Natile,[||] and Luigi G. Marzilli*,[†,§]

Contribution from the Department of Chemistry, Louisiana State University, Baton Rouge, Louisiana 70803, Department of Biochemistry and Division of Cancer Biology and Department of Radiation Oncology, Emory University School of Medicine, Atlanta, Georgia 30322, Department of Chemistry, Emory University, Atlanta, Georgia 30322, and Dipartimento Farmaco-Chimico, Università degli Studi di Bari, 70125, Bari, Italy

Received May 11, 2005; E-mail: lmarzil@lsu.edu

Abstract: The N7−Pt−N7 adjacent G,G intrastrand DNA cross-link responsible for cisplatin anticancer activity is dynamic, promotes local "melting" in long DNA, and converts many oligomer duplexes to single strands. For 5′-d($A_1T_2G_3G_4G_5T_6A_7C_8C_9C_{10}A_{11}T_{12}$)-3′ (**G3**), treatment of the (**G3**)$_2$ duplex with five pairs of [**L**Pt(H_2O)$_2$]$^{2+}$ enantiomers (**L** = an asymmetric diamine) formed mixtures of **L**Pt−**G3** products (1 Pt per strand) cross-linked at G_3,G_4 or at G_4,G_5 in all cases. **L** chirality exerted little influence. For primary diamines **L** with bulk on chelate ring carbons (e.g., 1,2-diaminocyclohexane), the duplex was converted completely into single strands (G_3,G_4 coils and G_4,G_5 hairpins), exactly mirroring results for cisplatin, which lacks bulk. In sharp contrast, for secondary diamines **L** with bulk on chelate ring nitrogens (e.g., 2,2′-bipiperidine, **Bip**), unexpectedly stable duplexes having two platinated strands (even a unique G_3,G_4/G_4,G_5 heteroduplex) were formed. After enzymatic digestion of **Bip**Pt−**G3** duplexes, the conformation of the relatively nondynamic G,G units was shown to be head-to-head (HH) by HPLC/mass spectrometric characterization. Because the HH conformation dominates at the G,G lesion in duplex DNA and in the **Bip**Pt−**G3** duplexes, the stabilization of the duplex form only when the **L** nitrogen adducts possess bulk suggests that H-bonding interactions of the Pt−NH groups with the flanking DNA lead to local melting and to destabilization of oligomer duplexes. The marked dependence of adduct properties on **L** bulk and the minimal dependence on **L** chirality underscore the need for future exploration of the roles of the **L** periphery in affecting anticancer activity.

Introduction

Upon entering the cells of a germ cell tumor, the effective and widely used *cis*-diamminedichloroplatinum(II) (cisplatin) anti-cancer drug is solvated and then reacts with cellular DNA, creating an N7−Pt−N7 d(GpG) intrastrand cross-link as the most abundant DNA adduct (∼65%).[1−3] A good correlation exists between the extent of intrastrand cross-linking and treatment outcomes.[4] Creation of local helical distortions in cellular DNA by cisplatin adduct formation is followed by specific binding of some cellular proteins; this binding is probably crucial for cisplatin anticancer activity.[1,5−9] It is noteworthy that, in addition to the DNA damage, cisplatin treatment of cancer cells also induced hyperacetylation of histone H4.[10]

Acquired and intrinsic resistance of tumor cells to cisplatin has prompted an extensive search for a superior analogue.[11−13] Because DNA adducts formed by platinum compounds with other carrier ligands will influence the structural nature of the DNA distortion and very likely the molecular specificity of the protein−DNA interactions,[1,3,14,15] the carrier ligand will affect

[†] Louisiana State University.
[‡] Emory University School of Medicine.
[§] Emory University.
[||] Università degli Studi di Bari.

(1) Kartalou, M.; Essigmann, J. M. *Mutat. Res.* **2001**, *478*, 1−21.
(2) Fichtinger-Schepman, A. M. J.; van der Veer, J. L.; den Hartog, J. H. J.; Lohman, P. H. M.; Reedijk, J. *Biochemistry* **1985**, *24*, 707−713.
(3) Cohen, S. M.; Lippard, S. J. *Prog. Nucleic Acid Res. Mol. Biol.* **2001**, *67*, 93−130.
(4) Reed, E.; Ozols, R. F.; Tarone, R.; Yuspa, S. H.; Poirier, M. C. *Proc. Natl. Acad. Sci. U.S.A.* **1987**, *84*, 5024−5028.
(5) Zamble, D. B.; Mikata, Y.; Eng, C. H.; Sandman, K. E.; Lippard, S. J. *J. Inorg. Biochem.* **2002**, *91*, 451−462.
(6) Whitehead, J. P.; Lippard, S. J. *Met. Ions Biol. Syst.* **1996**, *32*, 687−726.
(7) Gelasco, A.; Lippard, S. J. *Biochemistry* **1998**, *37*, 9230−9239.
(8) Jung, Y.; Lippard, S. J. *Biochemistry* **2003**, *42*, 2664−2671.
(9) Zhai, X. Q.; Beckmann, H.; Jantzen, H. M.; Essigmann, J. M. *Biochemistry* **1998**, *37*, 16307−16315.
(10) Wang, D.; Lippard, S. J. *J. Biol. Chem.* **2004**, *279*, 20622−20625.
(11) Wong, E.; Giandomenico, C. M. *Chem. Rev.* **1999**, *99*, 2451−2466.
(12) Wei, M.; Cohen, S. M.; Silverman, A. P.; Lippard, S. J. *J. Biol. Chem.* **2001**, *276*, 38774−38780.
(13) Hambley, T. W. *Coord. Chem. Rev.* **1997**, *166*, 181−223.
(14) Jamieson, E. R.; Lippard, S. J. *Chem. Rev.* **1999**, *99*, 2467−2498.
(15) Luscombe, N. M.; Laskowski, R. A.; Thornton, J. M. *Nucleic Acids Res.* **2001**, *29*, 2860−2874.

the biological processes that mediate anticancer activity. Pt−DNA adducts formed by **L**PtX$_2$ compounds (**L** = carrier diamine ligand, X = leaving group) have received little attention as compared to adducts formed by cisplatin.[12,16,17] Knowledge of carrier-ligand effects on DNA properties should help in the design of better platinum-based drugs; however, progress has been hampered by difficulties encountered in interpreting the solution behavior of the adducts[16,18] and in isolating crystalline materials. Success in obtaining X-ray crystallographic information has come only after considerable effort.[19−25] A major component of this challenge of characterizing cisplatin adducts is their dynamic nature, which impedes both solution-state and (by obstructing crystal formation) solid-state studies. In addition, more global platinum-induced distortions in the vicinity of the lesion of oligonucleotide adducts cause local melting, thus destabilizing oligomer duplexes and fostering dynamic processes.[7,26−29]

The "head-to-head" (HH) conformer (Figure 1) is the predominant conformation of the cisplatin−DNA adduct[30] and the simple Pt**L**(d(GpG)) models (carrier ligand **L** = $(NH_3)_2$ and primary amines).[31−35] To obtain evidence for other conformers, we have studied adducts of short, single-stranded (ss) oligonucleotides by employing a "retro-modeling" approach; we use carrier ligands that concentrate bulk near the platinum coordination plane to slow the dynamic motion about the Pt−N7 bonds, thus allowing multiple conformers to coexist and interconvert slowly to reach equilibrium.[16,30,36−39] The retro-model ligands,

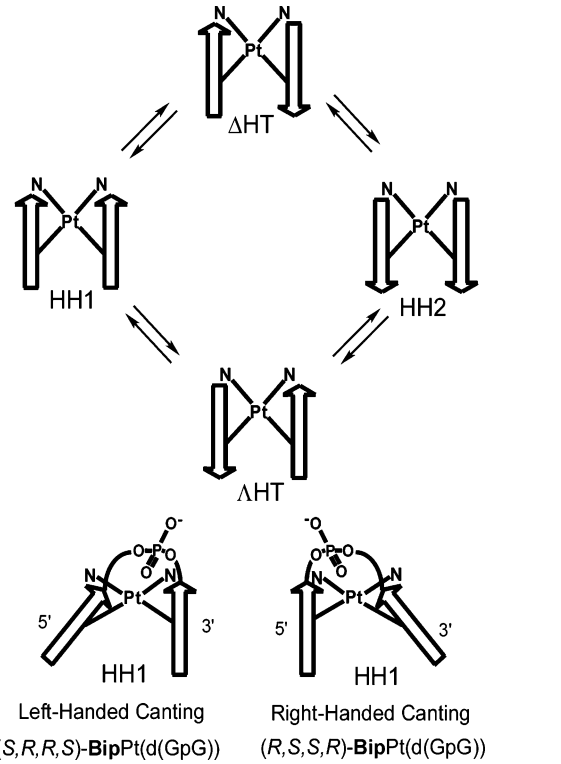

Figure 1. Top: Schematic representation of the interconversion between possible HT and HH atropisomers of PtG,G adducts viewed with the G coordination sites (5′-G left, 3′-G right) forward and carrier ligand N's to the rear (remainder of ligand omitted for clarity). Arrows represent the G bases with the tip of the arrow representing H8. The G conformation is anti except for a syn 3′-G in the ΔHT conformer (ΛHT, unknown). Bottom: Sketches of the HH1 rotamer of (*S*,*R*,*R*,*S*)- and (*R*,*S*,*S*,*R*)-**Bip**Pt(d(GpG)) with left-handed and right-handed canting, respectively, using arrows to represent G bases.

2,2′-bipiperidine (**Bip**) and *N*,*N*′-dimethyl-2,3-diaminobutane (**Me$_2$Dab**), in **Bip**PtX$_2$ and **Me$_2$Dab**PtX$_2$ have *S*,*R*,*R*,*S* or *R*,*S*,*S*,*R* configurations at the asymmetric N, C, C, and N chelate ring atoms (Figure 2).[16,37] The fairly rigid, three-ring **Bip**Pt unit decreases dynamic motion of **Bip**Pt adducts roughly one billion times relative to cisplatin adducts and about 100 times relative to **Me$_2$Dab**Pt adducts.[30,36−38,40−42] However, **Bip**Pt and **Me$_2$Dab**Pt adducts have very similar conformer distributions.

Two major products were found in each of the reactions of the enantiomers, [(*R*,*S*,*S*,*R*)-**Bip**Pt$(H_2O)_2]^{2+}$ and [(*S*,*R*,*R*,*S*)-**Bip**Pt$(H_2O)_2]^{2+}$, with d(GpG).[30,41] The new (*R*,*S*,*S*,*R*)-**Bip**Pt-(d(GpG)) conformer was also an HH conformer but with the opposite direction of propagation of the phosphodiester linkage from the normal HH conformer; we call the new conformer HH2 and the normal one HH1 (Figure 1). The new (*S*,*R*,*R*,*S*)-**Bip**Pt(d(GpG)) conformer is an unusual ΔHT (head-to-tail) adduct (Figure 1).[41]

Our objective was to determine the effects of carrier-ligand chirality and bulk on the form and properties of the DNA products. Toward this goal, we employed a self-complementary dodecamer containing two d($A_1T_2G_3G_4G_5T_6A_7C_8C_9C_{10}A_{11}T_{12}$) (**G3**) strands. Previous reactions of the (**G3**)$_2$ duplex with

(16) Ano, S. O.; Kuklenyik, Z.; Marzilli, L. G. In *30 Years of Cisplatin - Chemistry and Biochemistry of a Leading Anticancer Drug*; Lippert, B., Ed.; VHCH−Wiley−VCH: Basel, 1999; pp 247−291.
(17) Benedetti, M.; Malina, J.; Kasparkova, J.; Brabec, V.; Natile, G. *Environ. Health Perspect.* **2002**, *110 Suppl 5*, 779−782.
(18) Marzilli, L. G.; Saad, J. S.; Kuklenyik, Z.; Keating, K. A.; Xu, Y. *J. Am. Chem. Soc.* **2001**, *123*, 2764−2770.
(19) Sherman, S. E.; Gibson, D.; Wang, A. H. J.; Lippard, S. J. *J. Am. Chem. Soc.* **1988**, *110*, 7368−7381.
(20) Silverman, A. P.; Bu, W.; Cohen, S. M.; Lippard, S. J. *J. Biol. Chem.* **2002**, *277*, 49743−49749.
(21) Spingler, B.; Whittington, D. A.; Lippard, S. J. *Inorg. Chem.* **2001**, *40*, 5596−5602.
(22) Takahara, P. M.; Frederick, C. A.; Lippard, S. J. *J. Am. Chem. Soc.* **1996**, *118*, 12309−12321.
(23) Takahara, P. M.; Rosenzweig, A. C.; Frederick, C. A.; Lippard, S. J. *Nature* **1995**, *377*, 649−652.
(24) Ohndorf, U. M.; Rould, M. A.; He, Q.; Pabo, C. O.; Lippard, S. J. *Nature* **1999**, *399*, 708−712.
(25) Admiraal, G.; van der Veer, J. L.; de Graff, R. A.; den Hartog, J. H.; Reedijk, J. *J. Am. Chem. Soc.* **1987**, *109*, 592−594.
(26) Yang, D. Z.; van Boom, S. S. G. E.; Reedijk, J.; van Boom, J. H.; Farrell, N.; Wang, A. H. J. *Nat. Struct. Biol.* **1995**, *2*, 577−586.
(27) Coll, M.; Sherman, S. E.; Gibson, D.; Lippard, S. J.; Wang, A. H. J. *J. Biomol. Struct. Dyn.* **1990**, *8*, 315−330.
(28) Dunham, S. U.; Dunham, S. U.; Turner, C. J.; Lippard, S. J. *J. Am. Chem. Soc.* **1998**, *120*, 5395−5406.
(29) Mukundan, S., Jr.; Xu, Y.; Zon, G.; Marzilli, L. G. *J. Am. Chem. Soc.* **1991**, *113*, 3021−3027.
(30) Ano, S. O.; Intini, F. P.; Natile, G.; Marzilli, L. G. *J. Am. Chem. Soc.* **1998**, *120*, 12017−12022.
(31) Girault, J.-P.; Chottard, G.; Lallemand, J.-Y.; Chottard, J.-C. *Biochemistry* **1982**, *21*, 1352−1356.
(32) den Hartog, J. H. J.; Altona, C.; Chottard, J.-C.; Girault, J.-P.; Lallemand, J.-Y.; de Leeuw, F. A. A. M.; Marcelis, A. T. M.; Reedijk, J. *Nucleic Acids Res.* **1982**, *10*, 4715−4730.
(33) den Hartog, J. H. J.; Altona, C.; van Boom, J. H.; van der Marel, G. A.; Haasnoot, C. A. G.; Reedijk, J. *J. Am. Chem. Soc.* **1984**, *106*, 1528−1530.
(34) den Hartog, J. H. J.; Altona, C.; van der Marel, G. A.; Reedijk, J. *Eur. J. Biochem.* **1985**, *147*, 371−379.
(35) Kline, T. P.; Marzilli, L. G.; Live, D.; Zon, G. *J. Am. Chem. Soc.* **1989**, *111*, 7057−7068.
(36) Ano, S. O.; Intini, F. P.; Natile, G.; Marzilli, L. G. *Inorg. Chem.* **1999**, *38*, 2989−2999.
(37) Saad, J. S.; Scarcia, T.; Natile, G.; Marzilli, L. G. *Inorg. Chem.* **2002**, *41*, 4923−4935.
(38) Saad, J. S.; Scarcia, T.; Shinozuka, K.; Natile, G.; Marzilli, L. G. *Inorg. Chem.* **2002**, *41*, 546−557.
(39) Sullivan, S. T.; Saad, J. S.; Fanizzi, F. P.; Marzilli, L. G. *J. Am. Chem. Soc.* **2002**, *124*, 1558−1559.
(40) Ano, S. O.; Intini, F. P.; Natile, G.; Marzilli, L. G. *J. Am. Chem. Soc.* **1997**, *119*, 8570−8571.
(41) Marzilli, L. G.; Ano, S. O.; Intini, F. P.; Natile, G. *J. Am. Chem. Soc.* **1999**, *121*, 9133−9142.
(42) Marzilli, L. G.; Intini, F. P.; Kiser, D.; Wong, H. C.; Ano, S. O.; Marzilli, P. A.; Natile, G. *Inorg. Chem.* **1998**, *37*, 6898−6905.

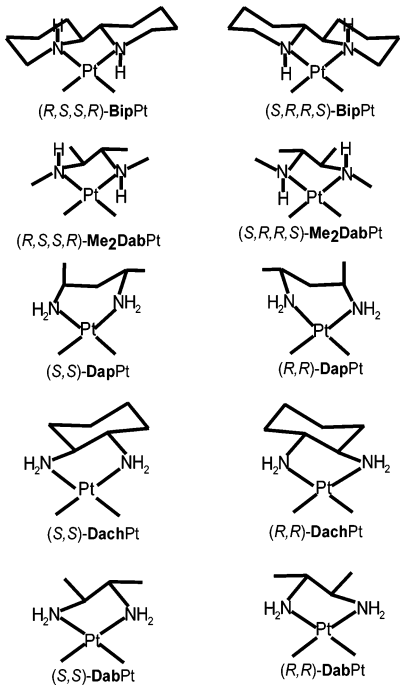

Figure 2. Sketches of the carrier ligands with *S*,*S* (left) and *R*,*R* (right) configurations of the C asymmetric centers. Top two rows show configurations for the asymmetric N centers (*R* on left and *S* on right): **Bip** = 2,2′-bipiperidine, **Me$_2$Dab**Pt = *N*,*N*′-dimethyl-2,3-diaminobutane, **Dap** = 2,4-diaminopentane, **Dach** = 1,2-diaminocyclohexane, and **Dab** = 2,3-diaminobutane. The order from top to bottom reflects the decreasing bulk that these ligands present to the DNA strands. **Dap** forms six-membered chelate rings, thus presenting somewhat greater bulk than **Dach** and **Dab**. These latter two primary diamine ligands form five-membered chelate rings and present similar bulk to the DNA.

cisplatin and **en**PtCl$_2$ (**en** = ethylenediamine)[43−46] gave ss products: G_4,G_5 adducts in a very stable hairpin form and G_3,G_4 adducts in a coil form.[43,46] In this work, we compare these products with those formed by (**G3**)$_2$ with the (*R*,*S*,*S*,*R*)- and (*S*,*R*,*R*,*S*)-enantiomers of [**Bip**Pt(H$_2$O)$_2$]$^{2+}$ and [**Me$_2$Dab**Pt(H$_2$O)$_2$]$^{2+}$ as well as the (*R*,*R*)- and (*S*,*S*)-enantiomers of [**Dach**Pt(H$_2$O)$_2$]$^{2+}$ (**Dach** = 1,2-diaminocyclohexane), [**Dap**Pt(H$_2$O)$_2$]$^{2+}$ (**Dap** = 2,4-diaminopentane), and [**Dab**Pt(H$_2$O)$_2$]$^{2+}$ (**Dab** = 2,3-diaminobutane) (Figure 2).

Experimental Section

Materials. G3 was synthesized at the Emory Microchemistry Facility by the phosphoramidate method and purified by ion exchange chromatography by using deionized water and 2 M NaCl (pH 6). Oligonucleotide concentrations were determined by UV spectroscopy: ϵ_{260} at 25 °C = 6300 M^{-1} cm^{-1} per base for **G3**.[46] Enantiomers of [**Bip**Pt(NO$_3$)$_2$] and [**Me$_2$Dab**Pt(H$_2$O)$_2$](NO$_3$)$_2$, synthesized as previously described,[30,47] were used to prepare 5 mM solutions of [**Bip**Pt(H$_2$O)$_2$]$^{2+}$ and 10 mM solutions of [**Me$_2$Dab**Pt(H$_2$O)$_2$]$^{2+}$ in deionized water for oligonucleotide reactions. Enantiomers of **Dach**PtCl$_2$, **Dap**PtCl$_2$, and **Dab**PtCl$_2$ were synthesized as described previously[48] and were converted to 10 mM diaqua species by the addition of 2.4 molar equiv of 10 mM AgNO$_3$. All other materials were obtained from commercial sources.

Reactions of (G3)$_2$ with Enantiomers of [LPt(H$_2$O)$_2$]$^{2+}$. In a typical reaction, an aqueous solution of (**G3**)$_2$ (2−4 mM in strands) was mixed in the dark at 4 °C with 1.5 equiv/strand of [**L**Pt(H$_2$O)$_2$]$^{2+}$, as described previously.[35,45] After 1−3 h, reaction mixtures were separated by denaturing gel electrophoresis as described previously;[46] gels were visualized by autoradiography, UV-shadowing, and/or ethidium bromide (EthBr) staining, and the ratio of adducts was determined using the Image Quant program. Reaction products were eluted from the gel, lyophilized, and stored at −20 °C or analyzed by nondenaturing gel electrophoresis.[46]

Modified Maxam−Gilbert Sequencing Reactions. Gel-eluted DNA adducts were 5′-end labeled and sequenced as described previously.[45,46] The products were separated on 20% denaturing polyacrylamide gels and analyzed by autoradiography.

Enzymatic Digestion of the BipPt−G3 Adducts. In a typical experiment, 10 nmol of platinated DNA was digested with nuclease P1 (NP1) (100 u) (Sigma, from *Penicillium citrinum*) and dephosphorylated with shrimp alkaline phosphatase (SAP) (50 u) (Promega) in the presence of 10 mM MgCl$_2$ and 50 mM CH$_3$COONa, pH = 5.5, in a total volume of 250 μL for 15−30 min. Products of the digest were analyzed by reverse-phase HPLC on a C-18 column (Agilent Technologies) by using 0.1 M ammonium acetate (pH = 6) (eluate A) and CH$_3$-CN:A in a 1:1 ratio (eluate B) and a gradient of 5−50% eluate B over either 20 or 30 min.

Mass Spectrometry. Electrospray mass spectrometry was performed at the Emory University Microchemical Facility. Products of the **Bip**Pt−**G3** digestion mixture were separated by HPLC as described above, collected manually, lyophilized, and stored at −20 °C. ESI-MS analysis was performed on a model API3000 triple-quadrupole mass spectrometer (PE-Sciex, Foster City, CA) equipped with a nano electrospray source (Protana, Odense, Denmark). MassChrom software v1.1 (PE-Sciex) was used to analyze the data. The HPLC fraction (1 μL) was diluted with 41 μL of 50% 2-propanol and transferred into a nanospray gold-coated needle. Typically, −800 V was applied to the spraying needle, the orifice was held at 70 V, and the focusing ring was held at 300 V. All other parameters were optimized during tuning and calibration of the instrument by using a manufacturer-recommended mixture of polypropylene glycols. The first quadrupole was scanned in the negative mode of operation from 500 to 1500 amu with 0.1-amu step and 1-ms dwell time. Detection of phosphate-containing species was accomplished by using the precursor ion scanning method and searching for precursors of the phosphate fragment ion (PO_3^-, −79 amu) in negative ion mode.[49] Conditions for precursor ion scanning were optimized by using bovine β-casein tryptic phosphopeptide [33−48] and synthetic flavine-adenine dinucleotide (Sigma) and were as follows: collision energy 120 eV and the collision gas flow at instrument setting 5.

Results

Electrophoretic Mobilities and Previous Relevant Studies. Size, charge, form, and shape influence electrophoretic mobility.[50] Even in the dilute conditions used in nondenaturing gel electrophoresis, the slower migrating (**G3**)$_2$ duplex dominates over a small equilibrium amount of a faster migrating **G3** ss hairpin.[46] Much higher concentrations, favoring the duplex, were used for reactions. Binding of cisplatin or aquated cisplatin converts the (**G3**)$_2$ duplex relatively cleanly into a mixture of a rapidly migrating ss hairpin (G_4,G_5 adduct) and a slightly slower

(43) Iwamoto, M.; Mukundan, S., Jr.; Marzilli, L. G. *J. Am. Chem. Soc.* **1994**, *116*, 6238−6244.
(44) Kline, T. P.; Marzilli, L. G.; Live, D.; Zon, G. *Biochem. Pharmacol.* **1990**, *40*, 97−113.
(45) Villanueva, J. M.; Jia, X.; Yohannes, P. G.; Doetsch, P. W.; Marzilli, L. G. *Inorg. Chem.* **1999**, *38*, 6069−6080.
(46) Yohannes, P. G.; Zon, G.; Doetsch, P. W.; Marzilli, L. G. *J. Am. Chem. Soc.* **1993**, *115*, 5105−5110.
(47) Xu, Y. H.; Natile, G.; Intini, F. P.; Marzilli, L. G. *J. Am. Chem. Soc.* **1990**, *112*, 8177−8179.
(48) Fanizzi, F. P.; Intini, F. P.; Maresca, L.; Natile, G.; Quaranta, R. *Inorg. Chim. Acta* **1987**, *137*, 45−51.
(49) Carr, S. A.; Huddleston, M. J.; Annan, R. S. *Anal. Biochem.* **1996**, *239*, 180−192.
(50) Offord, R. E. In *Methods Enzymol.*; Colowick, S. P., Kaplan, N. O., Eds.; Academic Press: New York, 1977; Vol. 46, pp 51−69.

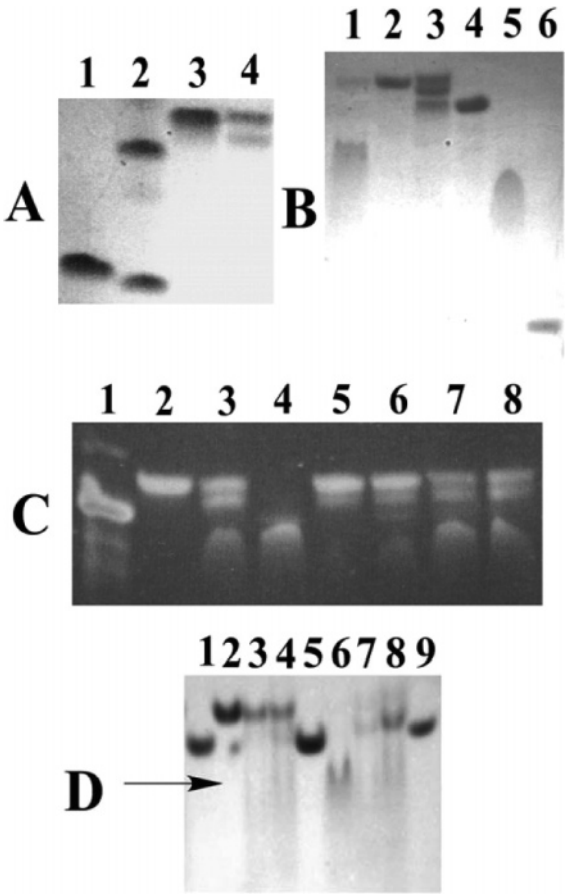

Figure 3. (A) UV shadowing analysis of a 20% denaturing polyacrylamide gel of the reaction of **G3** (lane 1) with *cis*-$[Pt(NH_3)_2(H_2O)_2]^{2+}$ (lane 2), with [(*R*,*S*,*S*,*R*)-[**Bip**$Pt(H_2O)_2]^{2+}$ (lane 3), and with [(*S*,*R*,*R*,*S*)-[**Bip**Pt-$(H_2O)_2]^{2+}$ (lane 4). (B) UV shadowing analysis of a 20% nondenaturing polyacrylamide gel of (*S*,*R*,*R*,*S*)-**Bip**Pt−**G3** G_3,G_4 and G_4,G_5 (lanes 1, 2), (*R*,*S*,*S*,*R*)-**Bip**Pt−**G3** (lane 3), purified $(\mathbf{G3})_2$ (lane 4), and *cis*-$Pt(NH_3)_2$−**G3** G_3,G_4 and G_4,G_5 (lanes 5, 6). (C) Ethidium bromide staining analysis of a 20% nondenaturing gel of $(\mathbf{G3})_2$ (lane 1), *R*,*S*,*S*,*R*-1 (lane 2), equilibrated *R*,*S*,*S*,*R*-2 (lane 3), *R*,*S*,*S*,*R*-3 (lane 4), *R*,*S*,*S*,*R*-1 + *R*,*S*,*S*,*R*-2 (lane 5), *R*,*S*,*S*,*R*-1 + *R*,*S*,*S*,*R*-3 (lane 6), *R*,*S*,*S*,*R*-2 + *R*,*S*,*S*,*R*-3 (lane 7), and (*R*,*S*,*S*,*R*)-**Bip**Pt−**G3** as isolated from a 20% denaturing gel (lane 8). (D) UV shadowing analysis of a 20% nondenaturing polyacrylamide gel of $(\mathbf{G3})_2$ (lanes 1, 5, and 9), the *S*,*R*,*R*,*S*-1 duplex (lanes 2, 3, and 4), and *S*,*R*,*R*,*S*-2 coil (lanes 6, 7, and 8) heated at 40 °C (aliquots in lanes 2, 6 taken at 0 h, in lanes 3, 7 taken at 24 h, and in lanes 4, 8 taken at 48 h). The arrow indicates coil mobility.

migrating ss coil form (G_3,G_4 adduct).[45,46] In preliminary work (unpublished) for these earlier investigations, we found that multiple adducts formed either if the reaction temperature was higher or if the 10-mer analogue with the central sequence of **G3** was used; because these are conditions favoring single strands, this is compelling evidence that the $(\mathbf{G3})_2$ duplex is the reactive form. Despite its lower charge, the faster mobility of the *cis*-$Pt(NH_3)_2$−**G3** hairpin than the **G3** hairpin was attributed to the *cis*-$Pt(NH_3)_2$−**G3** hairpin's compact structure.[43] Denaturing gels are buffered with high concentrations of urea, which disrupts most H-bonding interactions. **G3** has hairpin mobility in denaturing gels. Under denaturing conditions, coil and hairpin mobilities were found for the *cis*-$Pt(NH_3)_2$−**G3** G_3,G_4 and G_4,G_5 adducts, respectively, as found in nondenaturing gels.[45,46]

Reaction Products of $(G3)_2$ with $[BipPt(H_2O)_2]^{2+}$. A 1:3 ratio of $(\mathbf{G3})_2$:[**Bip**$Pt(H_2O)_2]^{2+}$ was used in these reactions. On denaturing gel, the (*R*,*S*,*S*,*R*)-**Bip**Pt−**G3** product gave one band

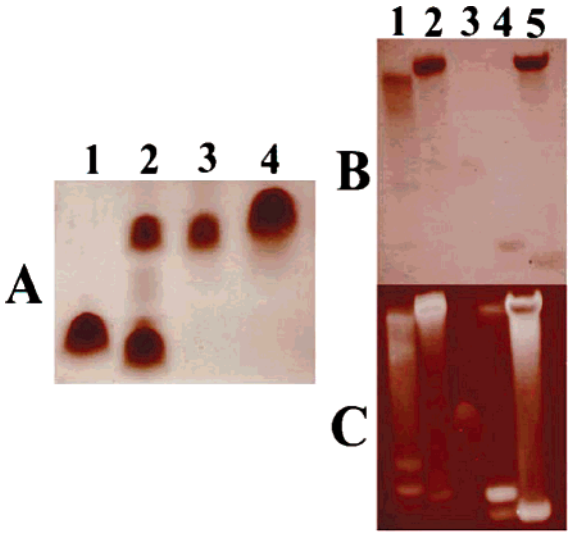

Figure 4. (A) UV shadowing analysis of a 20% denaturing polyacrylamide gel of the reaction of **G3** (lane 1) with *cis*-$[Pt(NH_3)_2(H_2O)_2]^{2+}$ (lane 2), [(*R*,*S*,*S*,*R*)-[**Me$_2$Dab**$Pt(H_2O)_2]^{2+}$ (lane 3), and [(*S*,*R*,*R*,*S*)-[**Me$_2$Dab**Pt-$(H_2O)_2]^{2+}$ (lane 4). (B) UV shadowing analysis and (C) ethidium bromide staining of a 20% nondenaturing polyacrylamide gel of (*S*,*R*,*R*,*S*)-**Me$_2$Dab**Pt−**G3** G_3,G_4/G_4,G_5 (lane 1), (*R*,*S*,*S*,*R*)-**Me$_2$Dab**Pt−**G3** G_3,G_4/G_4,G_5 (lane 2), *cis*-$Pt(NH_3)_2$−**G3** G_3,G_4 and G_4,G_5 (lanes 3, 4), and $(\mathbf{G3})_2$ (lane 5).

with coil mobility (Figure 3A, lane 3), whereas the (*S*,*R*,*R*,*S*)-**Bip**Pt−**G3** product yielded two bands with coil mobility (∼40:60 intensity ratio for the faster-migrating band:the slower-migrating band, Figure 3A, lane 4). **Bip**Pt−**G3** adducts were 5′-labeled and sequenced to determine the cross-link site. Only uncoordinated G's are methylated at N7 by dimethyl sulfate (DMS); thus, strand cleavage upon hot alkali treatment is observed for methylated (not platinated) G's. The (*R*,*S*,*S*,*R*)-**Bip**Pt−**G3** product (Figure 3A, lane 3) was found to cleave at both G_3 and G_5 (Supporting Information); this result, along with data below, shows that the one band found in denaturing gel electrophoresis is a mixture of the G_3,G_4 and G_4,G_5 adducts. Sequencing of the (*S*,*R*,*R*,*S*)-**Bip**Pt−**G3** adducts established that the slower and faster migrating bands had G_4,G_5 and G_3,G_4 cross-linked products, respectively (data not shown).

Reaction Products of $(G3)_2$ with $[Me_2DabPt(H_2O)_2]^{2+}$. In each of the reactions of (*R*,*S*,*S*,*R*)- or (*S*,*R*,*R*,*S*)-enantiomers of [**Me$_2$Dab**$Pt(H_2O)_2]^{2+}$, only one band with coil mobility was found in denaturing gels (Figure 4A, lanes 3 and 4). G-specific sequencing reactions revealed cleavage at G_5, but some cleavage occurred at G_3 as well (Supporting Information), indicating that both reactions formed a G_3,G_4 adduct and a less abundant G_4,G_5 adduct.

Reaction Products of $(G3)_2$ with $[DachPt(H_2O)_2]^{2+}$, $[DapPt(H_2O)_2]^{2+}$, or $[DabPt(H_2O)_2]^{2+}$. Both enantiomers of these $[LPt(H_2O)_2]^{2+}$ complexes gave two adducts with coil (slower) and hairpin (faster) mobilities in denaturing gels (Table 1), as reported for *cis*-$[Pt(NH_3)_2(H_2O)_2]^{2+}$.[45] The slower migrating **G3** adducts were found to have a G_3,G_4 cross-link, whereas the faster migrating adducts were found to have a G_4,G_5 cross-link, as evidenced by DMS strand cleavage only at G_5 or G_3, respectively. (An example of the Maxam−Gilbert sequencing gel of the (*R*,*R*)- and (*S*,*S*)-**Dach**Pt−**G3** adduct is shown in the Supporting Information.) In nondenaturing gels, the G_3,G_4 adducts found in the reaction of both enantiomers of [**Dach**Pt-$(H_2O)_2]^{2+}$, [**Dap**$Pt(H_2O)_2]^{2+}$, and [**Dab**$Pt(H_2O)_2]^{2+}$ had coil

Table 1. Form of **L**Pt−**G3** Based on Electrophoretic Mobilities

	adduct					
	G_3,G_4			G_4,G_5		
gel mobility:[a]	D	N-D	yield (%)	D	N-D	yield (%)
cis-$[Pt(NH_3)_2(H_2O)_2]^{2+}$	coil	coil	50	hairpin	hairpin	50
[(*R*,*S*,*S*,*R*)-**Bip**$Pt(H_2O)_2]^{2+}$	coil	duplex	50[b]	coil	duplex	50[b]
[(*S*,*R*,*R*,*S*)-**Bip**$Pt(H_2O)_2]^{2+}$	coil	duplex+coil	40	coil	duplex	60
[(*R*,*S*,*S*,*R*)-**Me$_2$Dab**$Pt(H_2O)_2]^{2+}$	coil	duplex	70[b]	coil	duplex	30[b]
[(*S*,*R*,*R*,*S*)-**Me$_2$Dab**$Pt(H_2O)_2]^{2+}$	coil	duplex/coil	70[b]	coil	duplex/coil	30[b]
[(*R*,*R*)-**Dach**$Pt(H_2O)_2]^{2+}$	coil	coil	55	hairpin	hairpin	45
[(*S*,*S*)-**Dach**$Pt(H_2O)_2]^{2+}$	coil	coil	30	hairpin	hairpin	70
[(*R*,*R*)-**Dap**$Pt(H_2O)_2]^{2+}$	coil	slow coil	40[c]	hairpin	hairpin	60[c]
[(*S*,*S*)-**Dap**$Pt(H_2O)_2]^{2+}$	coil	coil	35[c]	hairpin	hairpin	65[c]
[(*R*,*R*)-**Dab**$Pt(H_2O)_2]^{2+}$	coil	coil	35	hairpin	hairpin	65
[(*S*,*S*)-**Dab**$Pt(H_2O)_2]^{2+}$	coil	coil	35	hairpin	hairpin	65

[a] D = denaturing; N-D = nondenaturing. [b] Estimated by the extent of G-specific reaction in Maxam−Gilbert sequencing. [c] The related **Dap**$PtCl_2$ compound gave similar results.

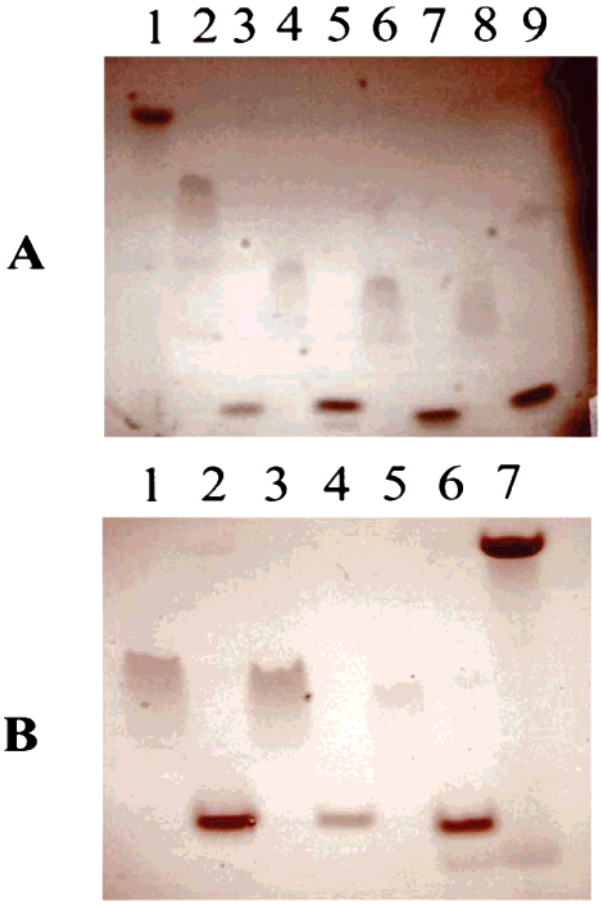

Figure 5. UV shadowing analysis of 20% nondenaturing polyacrylamide gels. (A) (**G3**)$_2$ (lane 1); (*R*,*R*)- and (*S*,*S*)-**Dap**Pt−**G3** G_3,G_4 (lanes 2, 4); (*R*,*R*)- and (*S*,*S*)-**Dap**Pt−**G3** G_4,G_5 (lanes 3, 5); (*R*,*R*)- and (*S*,*S*)-**Dab**Pt−**G3** G_3,G_4 (lanes 6, 8); and (*R*,*R*)- and (*S*,*S*)-**Dab**Pt−**G3** G_4,G_5 (lanes 7, 9). (B) (**G3**)$_2$ (lane 7); (*R*,*R*)- and (*S*,*S*)-**Dach**Pt−**G3** G_3,G_4 (lanes 1, 3); (*R*,*R*)- and (*S*,*S*)-**Dach**Pt−**G3** G_4,G_5 (lanes 2, 4); *cis*-$Pt(NH_3)_2$−**G3** G_3,G_4 (lane 5); and *cis*-$Pt(NH_3)_2$−**G3** G_4,G_5 (lane 6).

mobilities, and the G_4,G_5 adducts had hairpin mobilities (Figure 5A and B), the exception being the (*R*,*R*)-[**Dap**$Pt(H_2O)_2]^{2+}$ G_3,G_4 adduct, whose mobility was slower as compared to other coils (Figure 5A, lane 2). These data indicate that the structural deformation of DNA induced by the binding of these compounds is similar to that induced by cisplatin.

Duplex Form Dominates for BipPt−G3 Cross-Linked Adducts. The **Bip**Pt−**G3** products were purified by denaturing gel electrophoresis and loaded onto a nondenaturing gel to assess their forms under nondenaturing conditions. Controls having duplex ((**G3**)$_2$), coil (*cis*-$Pt(NH_3)_2$−**G3** G_3,G_4 adduct), and hairpin (*cis*-$Pt(NH_3)_2$−**G3** G_4,G_5 adduct) mobilities were loaded onto gels as well.

The (*R*,*S*,*S*,*R*)-**Bip**Pt−**G3** G_3,G_4/G_4,G_5 gel-purified product ran as three bands having duplex mobilities [labeled as *R*,*S*,*S*,*R*-1, *R*,*S*,*S*,*R*-2, and *R*,*S*,*S*,*R*-3, from slowest to fastest migration (Figure 3B, lane 3)]. In UV-shadowing analysis, the *R*,*S*,*S*,*R*-1 and *R*,*S*,*S*,*R*-2 bands were found to be about equally intense, while *R*,*S*,*S*,*R*-3 appeared to be slightly less intense (relative intensity 35:35:30). In nondenaturing gels, the (*S*,*R*,*R*,*S*)-**Bip**Pt−**G3** G_4,G_5 gel-purified band yielded only one band having duplex mobility (Figure 3B, lane 2), whereas the (*S*,*R*,*R*,*S*)-**Bip**Pt−**G3** G_3,G_4 adduct formed two bands, (*S*,*R*,*R*,*S*-1) and (*S*,*R*,*R*,*S*-2), having duplex and coil mobilities, respectively (Figure 3B, lane 1).

Each of the three (*R*,*S*,*S*,*R*)-**Bip**Pt−**G3** duplex bands was isolated from nondenaturing gel and loaded onto another 20% nondenaturing gel to determine whether any of the forms would equilibrate. *R*,*S*,*S*,*R*-1 and *R*,*S*,*S*,*R*-3 retained their original duplex mobilities, and each remained one band (Figure 3C, lanes 2 and 4, respectively). In contrast, *R*,*S*,*S*,*R*-2 redistributed to all three duplexes, exhibiting three bands (Figure 3C, lane 3). These data demonstrate that *R*,*S*,*S*,*R*-2 contains components of both *R*,*S*,*S*,*R*-1 and *R*,*S*,*S*,*R*-3. *R*,*S*,*S*,*R*-1, *R*,*S*,*S*,*R*-2, and *R*,*S*,*S*,*R*-3 were subjected to Maxam−Gilbert sequencing. The *R*,*S*,*S*,*R*-1 and the *R*,*S*,*S*,*R*-3 duplexes were found to contain only G_3,G_4 strands and only G_4,G_5 strands, respectively (Supporting Information). In contrast, *R*,*S*,*S*,*R*-2 cleaved at both G_3 and G_5 (Supporting Information), establishing that the *R*,*S*,*S*,*R*-2 duplex is a heteroduplex composed of one G_3,G_4 strand and one G_4,G_5 strand.

The (*S*,*R*,*R*,*S*)-**Bip**Pt−**G3** G_4,G_5 duplex retained its duplex mobility after isolation from nondenaturing gel and loading onto a new nondenaturing gel (data not shown). The **Bip**Pt−**G3** G_3,G_4 *S*,*R*,*R*,*S*-1 and *S*,*R*,*R*,*S*-2 bands also maintained their original duplex and coil mobilities, respectively. After isolation of the bands, neither of the two (*S*,*R*,*R*,*S*)-**Bip**Pt−**G3** duplexes converted to an ss form, suggesting that the duplexes are relatively stable under the isolation and subsequent electrophoresis conditions. After either the *S*,*R*,*R*,*S*-1 or the *S*,*R*,*R*,*S*-2 product was heated at 40 °C for 2 days, the nondenaturing gel revealed the presence of the other band (Figure 3D). The

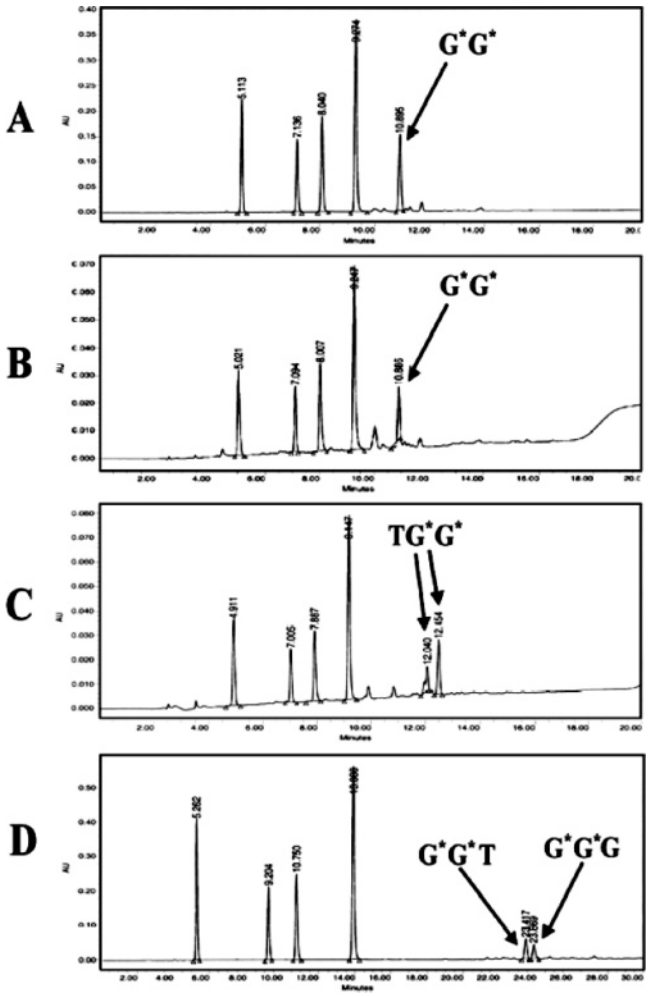

Figure 6. HPLC chromatograms of digestion mixtures of (A) (*S*,*R*,*R*,*S*)-**Bip**Pt−**G3** G_4,G_5 duplex, (B) (*S*,*R*,*R*,*S*)-**Bip**Pt−**G3** G_3,G_4 duplex, (C) (*S*,*R*,*R*,*S*)-**Bip**Pt−**G3** G_3,G_4 coil, and (D) (*R*,*S*,*S*,*R*)-**Bip**Pt−**G3** reaction product isolated from a denaturing gel. Fractions were identified by electrospray mass spectrometry and by running HPLC standards. Buffer A, 0.1 M ammonium acetate (pH = 6); buffer B, CH_3CN:A in 1:1 ratio. Gradient 5−50% eluate B over 20 (A, B, and C) or 30 min (D). G* represents platinated guanine.

S,*R*,*R*,*S*-2 coil product converted mostly to the *S*,*R*,*R*,*S*-1 duplex product, while only a small amount of the latter converted to the *S*,*R*,*R*,*S*-2 coil product. This conversion of the *S*,*R*,*R*,*S*-2 coil to the *S*,*R*,*R*,*S*-1 duplex (and vice versa) is consistent with the conclusion that these G_3,G_4 adducts differ principally in the conformation of the cross-link.

Enzymatic Digestion of the (*S*,*R*,*R*,*S*)-BipPt−G3 Adducts Reveals the Presence of the ΔHT Conformation in One G_3,G_4 Product. By using NP1 and SAP enzymes, we digested and dephosphorylated the (*S*,*R*,*R*,*S*)-**Bip**Pt−**G3** G_3,G_4 (*S*,*R*,*R*,*S*-1 duplex and *S*,*R*,*R*,*S*-2 coil) and G_4,G_5 (duplex) adducts to determine their nature. Digestion mixtures were then separated by HPLC, and the peaks were assessed by running HPLC standards and by mass spectrometry (Figure 6). All of the digestion product peaks were identified; these were dG, dC, dA, dT, and digestion products containing platinum (see below).

For the (*S*,*R*,*R*,*S*)-**Bip**Pt−**G3** G_3,G_4 adduct with coil mobility (*S*,*R*,*R*,*S*-2 product), simultaneous digestion and dephosphorylation (30 min) yielded two new HPLC peaks, both with mass corresponding to an (*S*,*R*,*R*,*S*)-**Bip**Pt−d(TpGpG) adduct (Figure 6C). The retention times of the two (*S*,*R*,*R*,*S*)-**Bip**Pt−d(TpGpG) HPLC peaks matched the retention times of those of the conformers formed in the reaction of d(TpGpG) and [(*S*,*R*,*R*,*S*)-**Bip**Pt$(H_2O)_2]^{2+}$. NMR methods have shown that the HH1 and ΔHT (*S*,*R*,*R*,*S*)-**Bip**Pt−d(TpGpG) conformers are formed (unpublished data). Because the ΔHT conformer converts slowly to the HH1 conformer in both **Bip**Pt−d(GpG)[41] and **Bip**Pt−d(TpGpG) adducts and because the (*S*,*R*,*R*,*S*)-**Bip**Pt−d(TpGpG) HH1 conformer is the highly favored thermodynamic product, it is clear that the presence of the (*S*,*R*,*R*,*S*)-**Bip**Pt−d(TpGpG) ΔHT conformer after digestion means that the cross-link in the *S*,*R*,*R*,*S*-2 coil has the ΔHT conformation. In other words, we attribute the presence of the HH1 conformer after digestion to the slow conversion of the ΔHT conformer to the HH1 conformer, a process that we have found to occur in all small d(GpG) retro-model adducts.[39] The fact that the cross-link of the *S*,*R*,*R*,*S*-2 coil has the ΔHT conformation indicates that this conformation destabilizes the duplex form otherwise favored by the bulky **Bip** ligands. In contrast, digestion of the (*S*,*R*,*R*,*S*)-**Bip**Pt−**G3** G_4,G_5 duplex and of the *S*,*R*,*R*,*S*-1 (G_3,G_4) duplex produced only the (*S*,*R*,*R*,*S*)-**Bip**Pt−d(GpG) HH1 conformer, indicating that only the HH1 conformer was present and that the HH1 conformer favors the duplex form.

(*R*,*S*,*S*,*R*)-BipPt−G3 Adducts Are Formed with Only the HH1 Conformation at the Pt−d(GpG) Binding Site. The reaction of [(*R*,*S*,*S*,*R*)-**Bip**Pt$(H_2O)_2]^{2+}$ and $(\mathbf{G3})_2$ gave three closely spaced duplex bands on nondenaturing gel electrophoresis, designated as *R*,*S*,*S*,*R*-1, *R*,*S*,*S*,*R*-2, and *R*,*S*,*S*,*R*-3 (see above). The **Bip** ligand prevents formation of the hairpin form, and both G_3,G_4 and G_4,G_5 strands are coils on denaturing gel electrophoresis (Figure 3A, lane 3 and Table 1), and because the strands have the same charge, only one band was observed. To obtain sufficient quantities of enzymatic digestion products for HPLC analysis, we chose to use denaturing gel electrophoresis followed by extraction of the one band that contained both G_3,G_4 and G_4,G_5 strands.

Digestion of this extract yielded two new HPLC peaks (Figure 6D) in addition to the HPLC peaks obtained after digestion of the $(\mathbf{G3})_2$ control. By using mass spectrometry to determine their molecular masses, the species in one peak summed to (*R*,*S*,*S*,*R*)-**Bip**Pt plus d(GpGpG), and the one in the other summed to (*R*,*S*,*S*,*R*)-**Bip**Pt plus d(GpGpT) or d(TpGpG). In the next paragraph, we explain how we used additional information to identify the products, including which G's are bound and the conformation of the cross-link.

We have previously found that in the retro models, if a residue 5′ to the Pt−d(GpG) cross-link is present, only the HH1 conformer is abundant enough to be detected clearly at equilibrium by NMR methods.[39] On the other hand, a residue 3′ to the Pt−d(GpG) cross-link allows formation of multiple conformers. When (*R*,*S*,*S*,*R*)-**Bip**Pt−d(GpGpG) and (*R*,*S*,*S*,*R*)-**Bip**Pt−d(GpGpT) enzymatic digestion products were heated for 2 days at 37 °C, both were found to undergo isomerization to a second conformer (data not shown). In contrast, adducts such as (*R*,*S*,*S*,*R*)-**Bip**Pt−d(TpGpG) did not isomerize under the same conditions. The isomerization of the (*R*,*S*,*S*,*R*)-**Bip**Pt−d(GpGpG) and (*R*,*S*,*S*,*R*)-**Bip**Pt−d(GpGpT) digestion products clearly indicates that they contain a nucleotide on the 3′ side of the Pt−d(GpG) cross-link. Undoubtedly, the two distinct adducts found in the digestion mixture arise from the two different strands. The (*R*,*S*,*S*,*R*)-**Bip**Pt−d(GpGpG) cross-link (with un-

digested G_5 on the 3′-side) is from the G_3,G_4 strand in the *R*,*S*,*S*,*R*-2 heteroduplex and the *R*,*S*,*S*,*R*-1 duplex, and the (*R*,*S*,*S*,*R*)-**Bip**Pt−d(GpGpT) cross-link (with undigested T_6 on the 3′-side) is from the G_4,G_5 strand in the *R*,*S*,*S*,*R*-3 duplex and the *R*,*S*,*S*,*R*-2 heteroduplex. HPLC comparisons of the (*R*,*S*,*S*,*R*)-**Bip**Pt−d(GpGpT) product from digestion of the (*R*,*S*,*S*,*R*)-**Bip**Pt−**G3** duplexes to the (*R*,*S*,*S*,*R*)-**Bip**Pt−d(GpGpT) NMR-characterized product of the reaction of d(GpGpT) with [(*R*,*S*,*S*,*R*)-**Bip**Pt$(H_2O)_2]^{2+}$ allowed us to establish unambiguously that the digestion product is the (*R*,*S*,*S*,*R*)-**Bip**Pt−d(GpGpT) HH1 conformer. (The second conformer formed on heating the digestion product is the (*R*,*S*,*S*,*R*)-**Bip**Pt−d(GpGpT) HH2 conformer.) These findings are all consistent with the presence of only one dominant conformation (HH1) at the two d(GpG)−Pt binding sites in the three (*R*,*S*,*S*,*R*)-duplexes.

Both Duplex and Coil Forms Exist for the Me$_2$DabPt−G3 Cross-Linked Adducts. Both the reaction of (*R*,*S*,*S*,*R*)-[**Me$_2$Dab**Pt$(H_2O)_2]^{2+}$ with (**G3**)$_2$ and the reaction of (*S*,*R*,*R*,*S*)-[**Me$_2$Dab**Pt$(H_2O)_2]^{2+}$ with (**G3**)$_2$ produced one band with coil mobility on denaturing gels. The adducts formed in each reaction contained a mixture of G_3,G_4 and G_4,G_5 products. The isolated band from the reaction of each enantiomer of [**Me$_2$Dab**Pt-$(H_2O)_2]^{2+}$ with (**G3**)$_2$ was loaded onto a 20% nondenaturing gel. The (*S*,*R*,*R*,*S*)-**Me$_2$Dab**Pt−**G3** adduct appeared as a smear spanning duplex and coil mobilities (Figure 4B and C, lane 1). Such behavior indicates that several forms exist for the (*S*,*R*,*R*,*S*)-**Me$_2$Dab**Pt−**G3** adduct and that these forms interconvert at a rate affecting mobility during the electrophoresis experiment. It is likely that this behavior is linked to an exchange between conformers of a given G,G product. In contrast, the (*R*,*S*,*S*,*R*)-**Me$_2$Dab**Pt−**G3** adduct ran as one band with duplex mobility (Figure 4B and C, lane 2), indicating that both the G_3,G_4 and the G_4,G_5 products strongly prefer the duplex form.

Discussion

Replacing the NH groups of cisplatin with substituents usually lowers anticancer activity.[13] Although this relationship has led to the obvious hypothesis that NH groups are needed for hydrogen-bonding interactions, we note that such substitutions of NH groups of the carrier ligand necessarily increase steric bulk. This increased bulk can alter the interactions of proteins and enzymes with DNA adducts having an HH1 cross-link. Furthermore, our recent studies with short ss oligonucleotides demonstrate that an increase in bulk can influence the nature and lifetime of conformations at the Pt−d(GpG) binding site.[16,30,36,41] Non-HH1 conformers should influence DNA repair or DNA−protein interactions; the carrier ligand could thereby affect the anticancer activity of Pt compounds by altering the cross-link conformation. However, when we began this work, it was not known whether such unusual conformers can form and be detectable only in the short ss oligonucleotides (∼6-mer), or if they can form and be detected in duplexes as well as in longer (>10-mer) oligonucleotides.

A Unique, Stable G_3,G_4/G_4,G_5 Heteroduplex. The *cis*-Pt$(NH_3)_2$−**G3** products were easily separated because on both denaturing and nondenaturing gels the G_3,G_4 product is a coil and the G_4,G_5 product is a hairpin (Table 1).[45,46] In contrast, we were unable to separate the (*R*,*S*,*S*,*R*)-**Bip**Pt−**G3** products by denaturing gel electrophoresis because both are coil forms. Obviously, the (*R*,*S*,*S*,*R*)-**Bip** ligand destabilizes the hairpin form. On nondenaturing gels, three distinct (*R*,*S*,*S*,*R*)-**Bip**Pt−**G3** duplex bands could be separated: *R*,*S*,*S*,*R*-1, *R*,*S*,*S*,*R*-2, and *R*,*S*,*S*,*R*-3. The (*R*,*S*,*S*,*R*)-**Bip** ligand stabilized the duplex form over both the coil and the hairpin forms. The isolated *R*,*S*,*S*,*R*-2 duplex was found to equilibrate to all three duplexes (Figure 3C, lane 3). Furthermore, the *R*,*S*,*S*,*R*-2 duplex formed when the isolated *R*,*S*,*S*,*R*-1 and *R*,*S*,*S*,*R*-3 duplexes were combined (Figure 3C, lane 6). These results indicate that one strand with a G_3,G_4 cross-link can form a duplex with one strand of a G_4,G_5 cross-link. To our knowledge, this is the first example of such a heteroduplex. Also, this is the first clear case in which the diamine carrier ligand appears to be able to control the preferred form of an oligonucleotide because neither of the *cis*-Pt$(NH_3)_2$−**G3** adducts is a duplex.[45,46]

The (G3)$_2$ Duplex Forms Only the HH1 Conformer When Treated with [(*R*,*S*,*S*,*R*)-BipPt$(H_2O)_2]^{2+}$. Only the HH1 conformer was found in the (*R*,*S*,*S*,*R*)-**Bip**Pt−**G3** adducts. In previous retro-model studies, multiple conformers were formed, especially as kinetic products.[39,41] (*R*,*S*,*S*,*R*)-**Bip**Pt−G,G adducts typically form HH1 and HH2 conformers (Figure 1).[30,39] For the HH2 conformer to form from a duplex, both G bases would have to rotate. The resulting disruptions of base stacking and of base pairing for two base pairs are obviously unfavorable processes and explain why no HH2 conformer was detected even as a kinetic product in the reaction of [(*R*,*S*,*S*,*R*)-**Bip**Pt-$(H_2O)_2]^{2+}$ with (**G3**)$_2$ (30 min of digestion is not sufficient time for HH1 to HH2 conversion of (*R*,*S*,*S*,*R*)-**Bip**Pt−d(GpG)). Perhaps most important, the absence of the HH2 form confirms the previous conclusion that the reactive form of the oligomer is the (**G3**)$_2$ duplex.

The greater stability of the duplex form, including the heteroduplex, over both the hairpin and coil forms when the cross-linking component is the bulky [(*R*,*S*,*S*,*R*)-**Bip**Pt$]^{2+}$ moiety can be understood in the context of three factors associated with the (*R*,*S*,*S*,*R*)-**Bip** carrier ligand. These factors are as follows: a chirality favoring right-handed HH1 canting (the canting direction in the duplex form of adducts, Figure 1); steric shielding of the positive Pt center and the NH groups (eliminating interactions favoring the coil form); and steric clashes between the piperidine rings and the flanking DNA that disfavor the hairpin. A more complete discussion of these factors follows our analysis of the other results in this study. The [(*S*,*R*,*R*,*S*)-**Bip**Pt$]^{2+}$ moiety differs from the [(*R*,*S*,*S*,*R*)-**Bip**Pt$]^{2+}$ moiety only in favoring left-handed HH1 canting (the typical canting direction in the ss form of adducts, Figure 1).

(*S*,*R*,*R*,*S*)-BipPt−G3 Duplexes Have the HH1 Conformation. The (*S*,*R*,*R*,*S*)-**Bip**Pt−**G3** G_4,G_5 adduct exists as only one detectable form, a stable duplex (Figure 3B, lane 2). Under the same conditions, the G_4,G_5 adduct of cisplatin formed a stable, tight hairpin. Thus, this result is consistent with those just reviewed for the G_4,G_5 adduct of the other **Bip** enantiomer, (*R*,*S*,*S*,*R*)-**Bip**. Only the HH1 conformer is present in the (*S*,*R*,*R*,*S*)-**Bip**Pt−**G3** G_4,G_5 duplex. To reiterate, this difference between the *cis*-Pt$(NH_3)_2$ and the **Bip**Pt adducts indicates that the size of a carrier ligand can dramatically influence the form of the cross-linked DNA product.

In contrast to the finding of only the duplex form with the G_4,G_5 product, the (*S*,*R*,*R*,*S*)-**Bip**Pt−**G3** G_3,G_4 cross-linked product has two different forms: a duplex (*S*,*R*,*R*,*S*-1), discussed here, and a coil, discussed below. As found for the (*S*,*R*,*R*,*S*)-

BipPt−**G3** G_4,G_5 product, only the HH1 digestion product was observed for the *S*,*R*,*R*,*S*-1 G_3,G_4 duplex. It is important to note that both (*S*,*R*,*R*,*S*)-**Bip**Pt−**G3** products (one G_3,G_4 and one G_4,G_5 product) having the cross-link in the HH1 conformation were exclusively in the duplex form. The **Bip** chirality in (*S*,*R*,*R*,*S*)-**Bip**Pt adducts favors L canting (Figure 1), and L canting is the canting direction favored by most ss G,G oligonucleotide adducts. Thus, of the three features influencing the form of the DNA adduct mentioned above, **Bip** ligand chirality is least important.

An Unusual ΔHT Cross-Link Conformation in the (*S*,*R*,*R*,*S*)-BipPt−G3 Coil. After digestion and dephosphorylation of the (*S*,*R*,*R*,*S*)-**Bip**Pt−**G3** G_3,G_4 coil (*S*,*R*,*R*,*S*-2), HPLC peaks were detected for both ΔHT and HH1 (*S*,*R*,*R*,*S*)-**Bip**Pt−d(TpGpG) conformers. Because the *S*,*R*,*R*,*S*-2 coil is a single species and because the ΔHT (*S*,*R*,*R*,*S*)-**Bip**Pt−d(TpGpG) conformer is thermodynamically very unstable, the *S*,*R*,*R*,*S*-2 coil must contain only a kinetically favored ΔHT cross-link. The (*S*,*R*,*R*,*S*)-**Bip**Pt−d(TpGpG) HH1 conformer detected after digestion of the *S*,*R*,*R*,*S*-2 coil must arise from conversion of the (*S*,*R*,*R*,*S*)-**Bip**Pt−d(TpGpG) ΔHT conformer to the thermodynamically favored HH1 (*S*,*R*,*R*,*S*)-**Bip**Pt−d(TpGpG) conformer. Conversion of the *S*,*R*,*R*,*S*-2 12-mer (ΔHT conformer) to largely the *S*,*R*,*R*,*S*-1 12-mer (HH1 conformer) (Figure 3 D) is expected, given the higher stability of the HH1 conformer when the cross-link has a 5′ residue.[39]

This *S*,*R*,*R*,*S*-2 product is a coil under nondenaturing conditions, even though every other product of the reaction of the $(\mathbf{G3})_2$ duplex with the $[\mathbf{Bip}Pt(H_2O)_2]^{2+}$ enantiomers is a duplex. However, the G,G conformation is HH1 in duplexes, but ΔHT in the *S*,*R*,*R*,*S*-2 coil, providing clear experimental evidence that the ΔHT cross-link conformation destabilizes the duplex form. We attribute this finding of the coil form for the *S*,*R*,*R*,*S*-2 product to the disruption of a GC base pair caused by the syn 3′-G conformation of the ΔHT conformer.[41,51] Local melting disrupts H-bonding and is more favorable at the G_3,G_4 site near the end of the $(\mathbf{G3})_2$ duplex than at the G_4,G_5 site closer to the middle of the $(\mathbf{G3})_2$ duplex. Thus, it is not too surprising that only the HH1 conformer was detected at the G_4,G_5 cross-link (Figure 6A) of the (*S*,*R*,*R*,*S*)-**Bip**Pt−**G3** G_4,G_5 adduct.

Consistency between the Results for the Me$_2$DabPt−G3 and the BipPt−G3 Adducts. As found for **Bip**Pt−**G3** adducts, both the G_3,G_4 and the G_4,G_5 adducts were found in the reactions of $(\mathbf{G3})_2$ with either enantiomer of $[\mathbf{Me_2Dab}Pt(H_2O)_2]^{2+}$. On nondenaturing gels, the (*R*,*S*,*S*,*R*)-**Me$_2$Dab**Pt−**G3** G_3,G_4/G_4,G_5 adducts had duplex mobility but moved as one band. Bands for the three possible duplexes (two homoduplexes and one heteroduplex) were not found (unlike the case of the (*R*,*S*,*S*,*R*)-**Bip**Pt−**G3** mixture of G_3,G_4 and G_4,G_5 adducts). Such a difference in properties of adducts containing **Me$_2$Dab**Pt and **Bip**Pt moieties has no precedent in studies of adducts with smaller G derivatives, which usually have very similar properties (conformer distributions, CD spectra, and chemical shifts for the G NMR signals).[37,38] However, the dynamic properties differ greatly, with the rate of conformer interconversion being more facile for **Me$_2$Dab** than for **Bip** analogues because rotation around the Pt−N7(G) bond is more rapid in **Me$_2$Dab**Pt adducts. This dynamic motion could facilitate the interchange of strands between duplexes if the rate of dissociation of the strands were facilitated by conformational flexibility at the cross-link. Also, if the (*R*,*S*,*S*,*R*)-**Me$_2$Dab**Pt−**G3** duplexes are thermodynamically less stable than the (*R*,*S*,*S*,*R*)-**Bip**Pt−**G3** duplexes, the concentration of single strands would be higher in the (*R*,*S*,*S*,*R*)-**Me$_2$Dab**Pt−**G3** adducts, a situation that facilitates interchange of strands between duplexes. Regardless of cause, the interchange of strands could rapidly equilibrate the three (*R*,*S*,*S*,*R*)-**Me$_2$Dab**Pt−**G3** duplexes, explaining the observation of only one band for the duplexes.

The (*S*,*R*,*R*,*S*)-**Me$_2$Dab**Pt−**G3** G_3,G_4/G_4,G_5 adducts both smeared in nondenaturing gels, indicating that the G_3,G_4 and G_4,G_5 adducts can adopt multiple forms that interconvert on a time scale resulting in smearing on the gel. The two enantiomers of $[\mathbf{Me_2Dab}Pt(H_2O)_2]^{2+}$ differ in stereochemistry, not in size. The (*S*,*R*,*R*,*S*)-**Me$_2$Dab**Pt−**G3** adducts are more dynamic than the (*S*,*R*,*R*,*S*)-**Bip**Pt−**G3** adducts. Because *S*,*R*,*R*,*S* chirality favors the ΔHT conformer and favors L canting in the HH1 conformation (Figure 1), a dynamic equilibrium would be expected to lead to a mixture of duplex (HH1) and coil (ΔHT) forms. Quite possibly, because **Me$_2$Dab** is smaller than **Bip**, two factors, *S*,*R*,*R*,*S* chirality favoring L canting typical of single strands and lower bulk favoring single strands (cf., next section), could both contribute to the lower stability of the duplex form for the (*S*,*R*,*R*,*S*)-**Me$_2$Dab**Pt−**G3** adducts. Thus, the results for the more dynamic **Me$_2$Dab**Pt adducts, confounded by dynamic motion, can nevertheless be rationalized by using the more definitive **Bip**Pt results.

Hairpin and Coil Forms of Adducts Having Primary Diamine Carrier Ligands with Steric Bulk on Asymmetric Chelate Ring Carbons. As mentioned, **L**Pt−**G3** adducts formed by the anticancer-active compounds, cisplatin and **en**$PtCl_2$, are not duplexes, but hairpin and coil forms for the G_4,G_5 and G_3,G_4 adducts, respectively.[45,46] Likewise, in nondenaturing gels the **L**Pt−**G3** adducts containing the six (*R*,*R*)- and (*S*,*S*)-**L**Pt (**L** = **Dach**, **Dap**, and **Dab**) moieties were all observed to exist in the hairpin form for the G_4,G_5 adducts and in the coil form for the G_3,G_4 adducts (Figure 5A and B, Table 1).

Influence of the Carrier Ligands on the Equilibrium Distribution. As just demonstrated, the carrier ligand influences which form is observed. The fact that G,G cross-linking of DNA by cisplatin lowers the melting temperature (T_m) of the DNA duplex is well documented.[52,53] The lower T_m indicates that denaturation of DNA is more favorable. Thus, relatively long pieces of DNA are needed for the duplex form to exist (typically at least an 8-mer). However, our work shows that the existence of the duplex form can depend greatly on the nature of the **L**Pt moiety. We believe that formation of a cross-link causes unfavorable interactions in the duplex and also makes favorable interactions weaker. The G base planes cannot be parallel in a **L**Pt−G,G intrastrand cross-link, with the effect that both base-stacking and base-pairing interactions will obviously be less favorable than in B-form DNA. However, denaturation is an equilibrium process, and, if the ss (coil or hairpin) forms also lose stabilizing interactions, the duplex form may still be more favored than either of the ss forms. Thus, we consider next the interactions of the carrier ligand with DNA in the various forms.

(51) Sullivan, S. T.; Ciccarese, A.; Fanizzi, F. P.; Marzilli, L. G. *J. Am. Chem. Soc.* **2001**, *123*, 9345−9355.
(52) Pilch, D. S.; Dunham, S. U.; Jamieson, E. R.; Lippard, S. J.; Breslauer, K. J. *J. Mol. Biol.* **2000**, *296*, 803−812.
(53) Poklar, N.; Pilch, D. S.; Lippard, S. J.; Redding, E. A.; Dunham, S. U.; Breslauer, K. J. *Proc. Natl. Acad. Sci. U.S.A.* **1996**, *93*, 7606−7611.

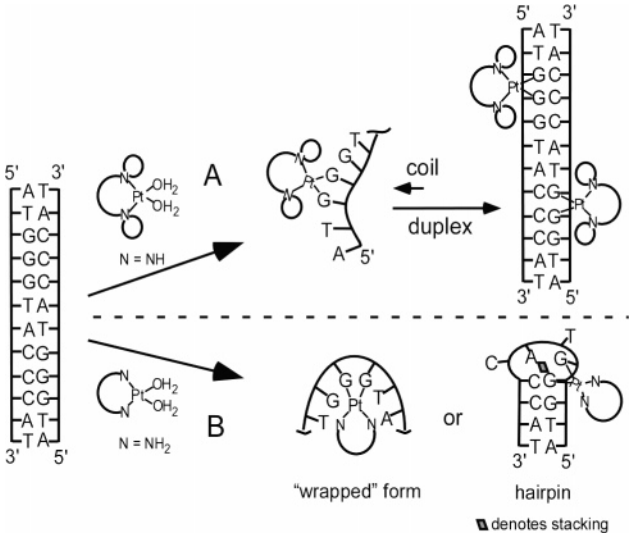

Figure 7. Scheme of $(\mathbf{G3})_2$ reactions with $[\mathbf{L}Pt(H_2O)_2]^{2+}$: (A) **L** = secondary diamines having steric bulk (represented with a small loop) on N atoms (the G,G adducts favor the duplex form, the homoduplexes not shown); (B) **L** = primary diamines lacking steric bulk on N atoms (the G_3,G_4 and G_4,G_5 adducts favor coil and hairpin forms, respectively). The large loop represents the carbon chain linking the two carrier-ligand N's.

DNA Interactions of the Carrier Ligands in the Duplex Form. Our discussion of the effect of the carrier ligand on the relative stability of the duplex, hairpin, and coil forms begins with our NMR-based model for a duplex containing the *cis*-$Pt(NH_3)_2$−G,G cross-link.[18] We created **Bip**Pt G,G duplex structural models by exchanging either enantiomer of the **Bip**Pt moiety for the *cis*-$Pt(NH_3)_2$ moiety in the duplex structural model. There was no difficulty in accommodating the **Bip** ligands, and also there is no obvious reason the **Bip**Pt−G,G cross-link would stabilize a duplex through carrier ligand−duplex interactions. Like the X-ray structure of an oligomer bound to an HMG protein,[24] the model used[18] has distortions mainly in the direction 5′ to the cross-link; thus, two cross-links in one duplex should be accommodated easily if the cross-links are on opposite strands because the region between the cross-links is 3′ to both cross-links. The unusual stability of the duplexes with one **L**Pt−G,G cross-link in each strand when **L** = **Bip** and not when **L** = primary diamine most likely arises from the lower stability of hairpin and coil ss forms when **L** = **Bip** (see next two sections).

In Figure 7, the sketch used to illustrate the duplex form shows the (*R*,*S*,*S*,*R*)-**Bip**Pt−**G3** heteroduplex as an example. Note that there are three base pairs between the cross-links. The G_3,G_4 and G_4,G_5 (*R*,*S*,*S*,*R*)-**Bip**Pt−**G3** homoduplexes have four and only two base pairs between the cross-links, respectively. The similar stabilities of these three (*R*,*S*,*S*,*R*)-**Bip**Pt−**G3** duplexes (cf., Figure 3) suggest that, in the region between the cross-links, base pairing is not weakened. However, qualitatively, the G_4,G_5 homoduplex, *R*,*S*,*S*,*R*-3, appears to be slightly less favored than the G_3,G_4 homoduplex, *R*,*S*,*S*,*R*-1, suggesting somewhat more distortion of the base pairs in the center of the G_4,G_5 homoduplex.

DNA Interactions of the Carrier Ligands in the Hairpin Form. It is quite striking that the six (*R*,*R*)- and (*S*,*S*)-**Dach**Pt−, **Dap**Pt−, and **Dab**Pt−**G3** G_4,G_5 hairpins share the high mobility of the *cis*-$Pt(NH_3)_2$−**G3** and **en**Pt−**G3** G_4,G_5 hairpins previously shown[43] to have an unusually compact structure (Figure 7B). As described above, we created **L**Pt−**G3** G_4,G_5 hairpin structural models by replacing **en** in the NMR-based **en**Pt−**G3** G_4,G_5 hairpin structural model[43] with other **L**'s. These models reveal no clashes involving the asymmetric carbon substituents and the nucleotide residues in or flanking the cross-link, consistent with the experimental finding that the six (*R*,*R*)- and (*S*,*S*)-**L**Pt−**G3** G_4,G_5 adducts adopt the compact hairpin form. Steric clashes between the NCH_2 groups of the (*R*,*S*,*S*,*R*)- and (*S*,*R*,*R*,*S*)-**Bip** ligands and neighboring sugars were evident in **Bip**Pt−**G3** hairpin models. Thus, it is apparent that the dramatic preference of **Bip**Pt and **Me$_2$Dab**Pt **G3** adducts with a G_4,G_5 cross-link to form duplexes and not hairpins is undoubtedly caused by the alkyl groups covalently linked to nitrogen atoms, not by substituents on the asymmetric carbons of the carrier-ligand chelate ring. In the next few paragraphs, we assess why the **Bip**Pt−**G3** G_4,G_5 adducts do not adopt the coil form.

DNA Interactions of the Carrier Ligands in the Coil Form. Some time ago, we investigated the unusual ^{31}P NMR signals in the **L**Pt−d(TCTCGGTCTC)) G,G type adduct (**L** = *cis*-$(NH_3)_2$ or **en**) and concluded that this ss type adduct was a distorted coil with the 5′ residues "wrapped around" the Pt binding site.[35] The negatively charged nucleotide sequences flanking the cross-link of a coil form "wrap around" the cationic *cis*-$[Pt(NH_3)_2]^{2+}$ or $[\mathbf{en}Pt]^{2+}$ moiety and possibly form hydrogen bonds to the Pt−NH groups.[35] The electrostatic and hydrogen-bonding interactions likely would distort the sugar phosphate backbone and explain the unusual ^{31}P NMR shifts. These "wrapped-around" interactions will stabilize the coil form especially because the NH groups are made into excellent H-bond donors by the electron-withdrawing Pt(II). Such "wrapping" of the cationic *cis*-$Pt(NH_3)_2$ moiety by flanking residues will result in more stable coils and in local "melted" regions of longer DNA, thereby decreasing the T_m of DNA.[52,53]

Such a "wrapped" ss coil form is undoubtedly less stable for the **Bip**Pt−**G3** and **Me$_2$Dab**Pt−**G3** adducts because both the **Bip** and the **Me$_2$Dab** carrier ligands are hydrophobic and bulky (Figure 2). In **Bip**Pt−**G3** adducts, the methylene-rich piperidine rings will prevent the flanking regions of the negative DNA strand from closely approaching the cationic Pt center (Figure 7).

The **Me$_2$Dab** ligand is less bulky than the **Bip** ligand but more bulky than the other carrier ligands studied in **L**Pt−**G3** G_3,G_4/G_4,G_5 adducts. Unlike these other adducts, the **Me$_2$Dab**Pt−**G3** G_3,G_4/G_4,G_5 adducts generally favor the duplex form. Consistent with the intermediate bulk of **Me$_2$Dab**, the (*S*,*R*,*R*,*S*)-**Me$_2$Dab**Pt−**G3** G_3,G_4/G_4,G_5 duplex appears to exist in part in a ss (most likely coil) form. The facts that (*S*,*R*,*R*,*S*)-**Me$_2$Dab**Pt chirality favors L canting and that this canting is characteristic of coils suggest a reasonable explanation for this result. The canting effect will favor the coil form. In contrast, the bulk effect, decreasing favorable interactions of the flanking negatively charged nucleotides with the cationic $[\mathbf{Me_2Dab}Pt]^{2+}$ moiety, should be less than for **Bip** adducts because the **Me$_2$Dab** carrier ligand is only moderately bulky. The net result will be a closer balance in stability between the duplex and coil forms, consistent with the results showing that the **Me$_2$Dab**Pt−**G3** adducts exist in the duplex form to a lesser extent than the **Bip**Pt−**G3** adducts.

Implications for Anticancer Activity. **L**Pt−**G3** adducts with **L** = $(NH_3)_2$ or a primary diamine, including carrier ligands

associated with anticancer activity, favor ss forms. In contrast, **L**Pt−**G3** adducts with **L** = *R*,*S*,*S*,*R*- and *S*,*R*,*R*,*S*-enantiomers of both **Bip**Pt and **Me$_2$Dab** associated with anticancer inactivity[17] favor the duplex form. The forms of **L**Pt−**G3** adducts are much more dependent on **L** bulk than on **L** chirality. However, when **L** = primary diamine, chirality is known to influence biological properties.[12,54] For example, (*R*,*R*)-**Dach**Pt(oxalato) (oxaliplatin) is used clinically to treat gastrointestinal tumors,[55] while its enantiomer, (*S*,*S*)-**Dach**Pt(oxalato), is not used in chemotherapy and is markedly more mutagenic.[48] The chiral components of the **Dach** ligand mainly project away from the DNA in a duplex. The differences in biological activity could result from differences in the interaction of the outer rim of a carrier ligand with cellular proteins, and the different biological effects observed for **Dach**Pt(oxalato) enantiomers do not necessarily require that the DNA adduct structure depend on **L** chirality. For example, differences in the thermodynamic destabilization and conformational distortions induced in DNA by intrastrand cross-links having the (*R*,*R*)-**Dab**Pt and (*S*,*S*)-**Dab**Pt moieties do not appear in sequences such as CGG (unpublished data), and only relatively small differences were noted in a DNA with the TGG sequence.[56] These different effects of **Dab** enantiomers, which may involve the T methyl group, were subtle and less dramatic than differences between the duplex, coil, and hairpin forms of DNA adducts reported here. Nevertheless, the reported dependence of properties on the configuration of chelate ring asymmetric carbons suggests the need for caution in extrapolating the current findings to other sequences.

We note that in our study the G_3,G_4 coil has the TGG sequence, and we find slower mobility for the (*R*,*R*)-**Dap**Pt−**G3** G_3,G_4 coil than for the (*S*,*S*)-**Dap**Pt−**G3** G_3,G_4 coil. Because the **Dap** ligand forms six-membered chelate rings, the alkyl substituents project more in the direction of the DNA than in the case of five-membered chelate rings. The **Dap** ligand appears to have a larger steric effect than the ligands associated with anticancer activity, such as **Dach**. This is an additional indication that **L** bulk might be associated with lower anticancer activity.

Conclusions

The presence of asymmetric carbon centers in the chelate rings of primary diamine ligands that form five-membered chelate rings has very little effect on the properties of our 12-mer oligonucleotide adducts bearing one Pt−G,G intrastrand cross-link. In contrast, replacing one of the NH groups on each nitrogen of diamines with an alkyl group leads to large differences in the properties of such 1:1 Pt:**G3** adducts. The most dramatic effect of adding bulk to the carrier ligand is the stabilization of the duplex form as compared to both the common (coil) and the uncommon (hairpin) ss forms. We attribute this unusual stability of the duplex form to unfavorable destabilizing interactions of the *N*-alkyl substituents with the flanking DNA of these ss forms rather than to any favorable stabilizing interactions of these groups with the flanking DNA in the duplex form.

The absolute configuration of the asymmetric carbon centers and of even the asymmetric nitrogen centers appears to have very little effect on the nature of the 12-mer adducts. Although the retro-modeling approach allowed us to establish that some non-HH1 conformer can form as a kinetic product in a duplex reaction, duplexes formed largely HH1 products even in cases of bulkier ligands. Thus, it appears likely that the differences in anticancer activity and mutagenicity observed for enantiomeric pairs of Pt drugs depend primarily on differences in biodistribution and differences in interactions of proteins with the chelate ring substituents. Differences in cross-link conformation are unlikely to be a major carrier-ligand-dependent factor affecting anticancer activity. Overall carrier-ligand bulk does have a major influence on adduct behavior; greater bulk favors the duplex over the ss forms. This preference was not sequence dependent; indeed, in one case a mixture of these strands produced an unusual heteroduplex.

Our studies indicate that a very significant and perhaps dominant factor leading to duplex destabilization by the *cis*-$Pt(NH_3)_2$−G,G intrastrand cross-link is the ability of the Pt−NH groups to stabilize the ss-like structures in the region of the cross-link and the flanking DNA. It is reasonable to hypothesize that the resulting ss character induced by the Pt−NH groups may be important in anticancer activity. The results obtained here suggest the need for studies directed at assessing the possible role of ss character of the DNA adduct during the biological process leading to cancer cell death.

Acknowledgment. This research was supported by NIH Grants GM29222 (to L.G.M.) and CA073041 (to P.W.D.), and by the University of Bari and MIUR (PRIN 2001 No. 2001053898). We thank Dr. Francesco P. Intini for the synthesis of the compounds, Dr. Malgorzata Lipowska for help with the HPLC experiments, and Dr. Frank Hubalek for help with mass spectrometry experiments. We thank Dr. Patricia Marzilli for helpful discussions, and Kristie Adams of the Marzilli lab for her assistance in manuscript submission.

Supporting Information Available: Autoradiograms of Maxam−Gilbert sequencing reactions. This material is available free of charge via the Internet at http://pubs.acs.org.

JA053089N

(54) Chaney, S. G.; Vaisman, A. *J. Inorg. Biochem.* **1999**, *77*, 71−81.
(55) Ramanathan, R. K.; Clark, J. W.; Kemeny, N. E.; Lenz, H. J.; Gococo, K. O.; Haller, D. G.; Mitchell, E. P.; Kardinal, C. G. *J. Clin. Oncol.* **2003**, *21*, 2904−2911.
(56) Malina, J.; Hofr, C.; Maresca, L.; Natile, G.; Brabec, V. *Biophys. J.* **2000**, *78*, 2008−2021.